Gümüşhane University Journal of Science

GUFBD / *GUJS* (2024) 14(2): 623-638 doi: 10.17714/gumusfenbil.1418085 Research Article

Numerical analysis of a mini wind tunnel and experimental investigation of the mini wind tunnel utilizing a portable, three-axis load/balance measurement system

Mini rüzgar tünelinin sayısal analizi ve taşınabilir, üç eksenli bir yük/denge ölçüm sistemi kullanılarak mini rüzgar tünelinin deneysel incelenmesi

Emre KARA*[1], Kübra ÖZTÜRK[1]

[1]*Gaziantep University, Faculty of Aeronautics and Aerospace, Aerospace Engineering Department, 27310, Gaziantep*

• Received: 11.01.2024 • Accepted: 02.05.2024

Abstract

Investigation of a portable three-axis load/balance measurement system in a mini wind tunnel is the main subject of study. Firstly, a mini wind tunnel is designed, numerically analyzed and constructed. Then, measurements of lift and drag forces on a selected airfoil are carried out using data from the measurement system located in the test area. Tri-axis load/balance measurement system developed has a total of three load cells, one for drag and two for lift. Sensor data acquisition codes are written using Ardunio and force measurement experiments are performed at various angles of attack on the NACA2412 airfoil at Reynolds number of 60000, for the maximum flow rate of 5200 m^3/h through fan controller in the constructed mini wind tunnel. After completing the mesh independence test, numerical studies are conducted in ANSYS Fluent for the same range of angles of attack using three different turbulence models. Realizable k-ε turbulence model gives more realistic high stall angles of attack than other turbulence models and similar to experimental results. In addition to the current experimental study, four other literature studies in similar Reynolds number ranges are used as reference cases. A visual study of the flow around the airfoil is given as velocity contours in addition to the numerical comparisons. From the numerical and experimental results, it is concluded that the NACA2412 airfoil profile wings are more efficient for moderate to high Reynolds numbers and the constructed load/balance measurement system and mini wind tunnel are highly successful in terms of lift and drag measurements.

Keywords: Computational fluid dynamics, Engineering design, Experimental investigation, Load/balance measurement system, Wind tunnel

Öz

Mini bir rüzgâr tünelinde taşınabilir üç eksenli yük/denge ölçüm sisteminin incelenmesi çalışmanın ana konusudur. İlk olarak, bir mini rüzgar tüneli tasarlanmış, sayısal olarak analiz edilmiş ve inşa edilmiştir. Ardından, test alanında bulunan ölçüm sisteminden elde edilen veriler kullanılarak seçilen bir kanat üzerindeki kaldırma ve sürükleme kuvvetlerinin ölçümleri gerçekleştirilmiştir. Geliştirilen üç eksenli yük/denge ölçüm sistemi, biri sürükleme ve ikisi kaldırma kuvveti için olmak üzere toplam üç yük hücresine sahiptir. Sensör veri toplama kodları Ardunio kullanılarak yazılmış ve inşa edilen mini rüzgar tünelinde NACA2412 kanat profili üzerinde çeşitli hücum açılarında, 60000 Reynolds sayısında, maksimum 5200 m^3/h debi için fan kontrolcüsü aracılığıyla kuvvet ölçüm deneyleri gerçekleştirilmiştir. Ağ bağımsızlık testi tamamlandıktan sonra, üç farklı türbülans modeli kullanılarak aynı hücum açısı aralığı için ANSYS Fluent'te sayısal çalışmalar yapılmıştır. Gerçekleştirilebilir k-ε türbülans modeli, deneysel sonuçlara benzer şekilde, diğer türbülans modellerine göre daha gerçekçi yüksek tutunma kaybı (perdövites) hücum açıları vermektedir. Mevcut deneysel çalışmaya ek olarak, benzer Reynolds sayısı aralıklarındaki diğer dört literatür çalışması referans vakalar olarak kullanılmıştır. Sayısal karşılaştırmalara ek olarak, kanat profili etrafındaki akışın görsel bir çalışması da hız konturları olarak verilmiştir. Sayısal ve deneysel sonuçlardan, NACA2412 kanat profilinin orta ve yüksek Reynolds sayıları için daha verimli olduğu ve kurulan yük/denge ölçüm sistemi ve mini rüzgar tünelinin kaldırma ve sürükleme kuvveti ölçümleri açısından oldukça başarılı olduğu sonucuna varılmıştır.

Anahtar kelimeler: *Hesaplamalı akışkanlar dinamiği, Mühendislik tasarımı, Deneysel inceleme, Yük/denge ölçüm sistemi, Rüzgar tüneli*

*Emre KARA; emrekara@gantep.edu.tr

1. Introduction

Wind tunnels, where pressure distribution, velocity characteristics and aerodynamic forces are measured, play a very important role in many areas, especially in the design process of an aircraft (Barlow et al., 1999). In general, wind tunnels can be considered as structures consisting of two subsystems: a subsystem that provides the air flow and a measurement system where the flow characteristics are measured.

In the field of aeronautics, wind tunnels are infrastructures used to test the interaction of objects with airflow. Aerodynamic investigations in design are carried out by numerical modelling, experimental work (wind tunnel tests) and flight tests/function tests. Wind tunnel testing is essential because the numerical modelling analysis of the airflow needs to be validated experimentally, while real-world testing can be complex, expensive and dangerous.

There are two basic types of wind tunnel, depending on how the airflow circulates: open circuit and closed circuit (Barlow et al. 1999). In an open circuit wind tunnel, air follows a straight path from the entrance region through the contraction to the test section, followed by a diffuser, a fan and the exhaust. These types of tunnels can have an open jet or Eiffel type test section with no solid boundaries or a closed jet or National Physical Laboratory (NPL) type test section with solid boundaries. A closed circuit wind tunnel, also known as a Prandtl or Gottingen type, has the air continuously recirculating with little or no exchange with the exterior. According to Barlow et al. (1999), both open- and closed-circuit and open- and closed-jet designs have advantages and disadvantages. In general, the available funds and the purpose can determine the type of tunnel chosen.

Measuring the total loads on a model in the wind tunnel is important for aerodynamic analysis as it predicts the performance of the model. Four different methods (Barlow et al. 1999) are commonly used to calculate the loads (specifically lift and drag forces) applied to a model in a wind tunnel:

- Direct measurement of load/balance,
- Indirect measurement of the pressure distribution on the surface of the model using holes connected to pressure gauges.
- Indirect measurement of stress distribution across the model using orifices or pressure/shear sensitive coatings.
- Calculation of forces from the equation of motion.

Currently, there are commercially available load/balance measurement system designs for wind tunnels (Ate AEROTECH, 2024) and portable aerodynamic measurement system designs for water tunnels (Koca, 2019). Wind tunnel load (force) balance designs begin with the very first wind tunnel designed in 1871 (Randers-Pehrson, 1935). Mr. Wenham's design uses a vertical steel spindle as the load balance. The design uses a vertical spring steelyard to measure lift and the steelyard connected to the vertical spindle by a lever to measure drag. The measurement procedure is not straightforward, i.e. the lift and drag readings are taken by two people simultaneously. The measurement systems are more compact and digitized in today's wind tunnels; however the procedure does not change. The following paragraphs summarise the load/balance measurement systems constructed for use in educational wind tunnels in the last 15 years:

In the 2009 study by Portman et al. (2009), the model is mounted in the wind tunnel using 6 degrees of freedom (DOF) isotropic force lines suspended in the wind tunnel. It has been found to be easier to calibrate than the external force balance system. However, it cannot be used in the design of a portable measurement system due to its fixed installation in the tunnel.

In the study by Samardžić et al. (2014), the tested model is mounted on a triangular platform with three connecting beams. The triangular platform is connected to three vertical and three horizontal load cells by beams at three corners. Therefore, with this test setup, measurements are made in six axes. This test setup can be used as a reference for future measurement systems, but six-axis load/balance measurement systems are outside the scope of the current study.

In a recent Master's thesis, Fernandes (2018) created a six-axis motion system and a measurement system using the "Stewart" platform. The Stewart platform (Stewart, 1965) is basically formed by connecting two 6-sided tables with rods. The upper table is smaller than the lower table. Ball joints are used to allow axial movement.

As this setup measures in six axes, it is not compatible with a three-axis measuring system, but can be used as a reference for future measuring systems.

In a recent bachelor thesis, Tintoré (2018) designed a three-axis wind tunnel force balance that is very similar to our approach. The study attempts to design a load/balance system for a small low speed wind tunnel capable of measuring lift, drag and pitching moment of small models. The advantages of the current study are the portability and compactness of the proposed measurement system compared to Tintoré's study. In addition, the current study will produce a mini wind tunnel compatible with the proposed measurement system.

Tomin et al. (2020) conducted a study to test the three-axis force balance and its potential for educational purposes, building on the work of Tintoré (2018). The authors aimed to provide a step-by-step guide for researchers to construct a load balance system. They generated aerodynamic data for a NACA 6412 foam wing with a 150 mm chord, using purely experimental methods.

Kumar et al. (2021) developed and calibrated a low-cost six-component wind tunnel balance, similar to Fernandes' (2018) design. They built a 22 kg Stewart platform to serve as the wind tunnel balance and calibrated it using four experimental designs: central composite design, Box-Behnken design, Box-Behnken design with two active filters for decoupling, and modern design of experiments. The authors concluded that the use of reduced order models can shorten calibration time. The paper focuses mainly on reduced order models for calibration rather than the design itself. One issue with the design is its weight, which makes it unsuitable for portability.

Similar to the above studies, there are many models of force/balance measurement systems for wind tunnels. In this study, the measurement system to be used will be more compact and portable, as the three-axis force measurement will be performed on an external balance that is compatible with the mini wind tunnel produced.

The aim of this study is to construct a low-cost mini wind tunnel and a compatible, low-cost load balance measurement system. Previous studies have focused on either building a wind tunnel or a load balance measurement system. However, in this study, both a wind tunnel and a load balance measurement system are developed from scratch. Additionally, a numerical virtual wind tunnel is also created.

In the following materials and methods section, firstly, the mini wind tunnel design is discussed both numerically and constructively. Secondly, the proposed requirements for the load/balance measurement system are summarized and the fabrication methods are given as a summary for both the load/balance measurement system and the mini wind tunnel design.

2. Materials and methods

2.1. Mini wind tunnel design procedures

In this study, a low-cost (nearly 300 $ including mini wind tunnel construction), portable and compact three-axis load/balance measurement system is constructed that can be adapted and used in wind tunnels of different sizes and characteristics for future academic use. The mini wind tunnel designed for this study is a suction-type, open-circuit, closed-jet wind tunnel, which is designed to meet the basic requirements of a load/balance measurement system and is also easier to manufacture than a closed-circuit wind tunnel. The tunnel consists of four main sections: The entrance section with a settling chamber, the test section, the diffuser and the fan (Figure 1). At the entrance, the settling chamber has a honeycomb structure that allows for streamlined flow. The chamber connects to the test section in a contracted path called the collector. The test section is the region where the experiments are carried out, so the design of the load/balance measurement system is located at the test section. The air is discharged through the diffuser by means of a suction fan located at the outlet section.

In this project, the load/balance measurement is designed to be portable for wind tunnels, adaptable for tunnels of different sizes and flexible to build alongside similar systems. In addition, the cost of commercial measurement systems is high compared to an engineered design. Direct load/balance measurement is selected in this study. This measurement method allows the direct measurement of forces by separating the components of forces with a system of equilibrium with respect to a specific reference system. As Tintore (2018) has stated, there are two types of balances used in load testing: external balances, which carry the loads outside the tunnel

before they are measured, and internal balances, which fit into the models. The NACA 2412 airfoil wing has a chord length of 100 mm and a maximum thickness of 12 mm. The load cells used for load balancing have dimensions of 81 x 13.5 x 13.5 mm. Due to the dimensions of the load cells, it is not feasible to use an internal balance system in the low-cost design. In another case, Barlow et al. (1999) state that external balances have a higher resolution and a greater ability to maintain their calibration over very long periods of time compared to internal balances. Therefore, it is more convenient to use external balance system in this study.

The first step in the current design study is to numerically design and build a simple mini wind tunnel. Secondly, the main subject of the study, the load/balance measurement system, is constructed and placed in the test section of the mini wind tunnel.

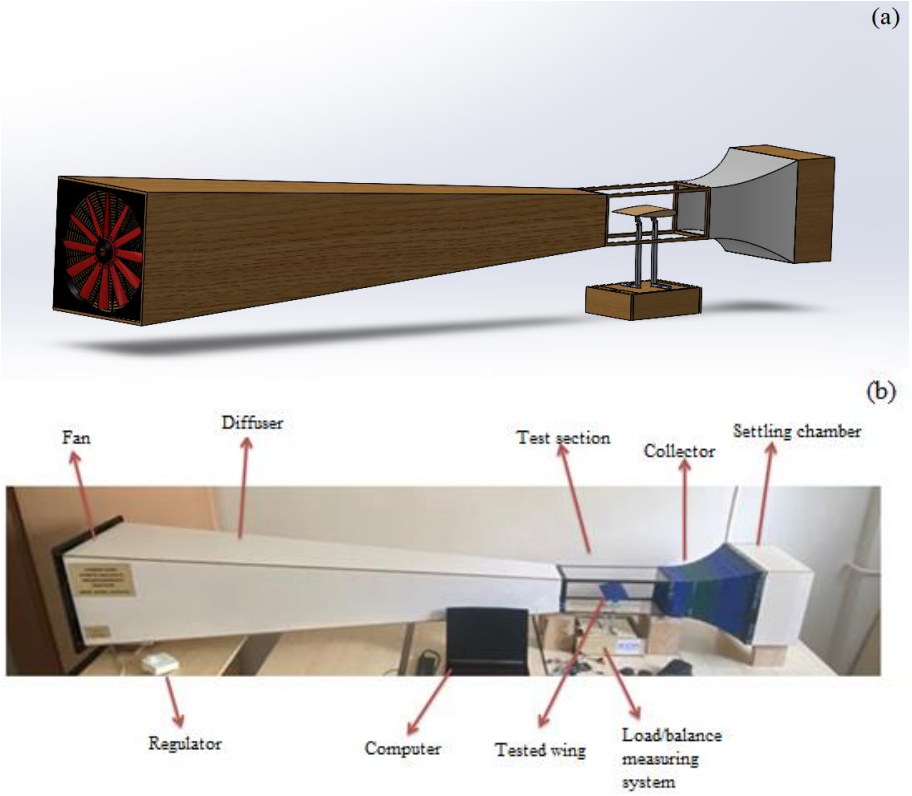

Figure 1. (a) Mini wind tunnel design, (b) the parts of the manufactured wind tunnel with tested wing and the load/balance measurement system

The steps in mini wind tunnel design can be summarized as follows:

- Using the general rules given in Barlow et al. (1999), the solid parts of the wind tunnel are designed in a SolidWorks CAD program. The dimensions of the wind tunnel are given in Figure 2.
- Prior to fabrication of the parts, the corresponding fluid (air) domain inside the wind tunnel is designed in ANSYS DesignModeler, meshed in ANSYS Meshing and the flow simulated in ANSYS Fluent computational fluid dynamics (CFD) solver for an inlet velocity of 3.4 m/s. 24 case studies (3 turbulence models × 8 angles of attack) are carried out to find the most appropriate turbulence model, namely Spalart-Allmaras, Realizable k-ε and Shear-Stress-Transport (SST) k-ω at angles of attack (α) of -4°, 0°, 4°, 8°, 12°, 16°, 18° and 20°. Details of the numerical design prior to these CFD procedures are given in Section 2.1.1.
- After the design of the load/balance measurement system (details are given in Section 2.1.2.), the design of the wind tunnel (Figure 1.b) is ensured to be the ultimate before the manufacturing steps.
- After numerical verification of low turbulence intensity (average 3%), streamlined flow in the range α = -4° to 20° inside the test section of the wind tunnel, the manufacturing processes are started.
- First, the honeycomb and the collector are fabricated in a 3D printer.
- The entrance area enclosing the honeycomb and the diffuser are made of wood material due to its lower cost and higher stiffness compared to sheet metal.

- The test section is made of transparent plexiglas material for flow visualization studies in future work.
- The fan with a regulator is mounted at the end of the diffuser.

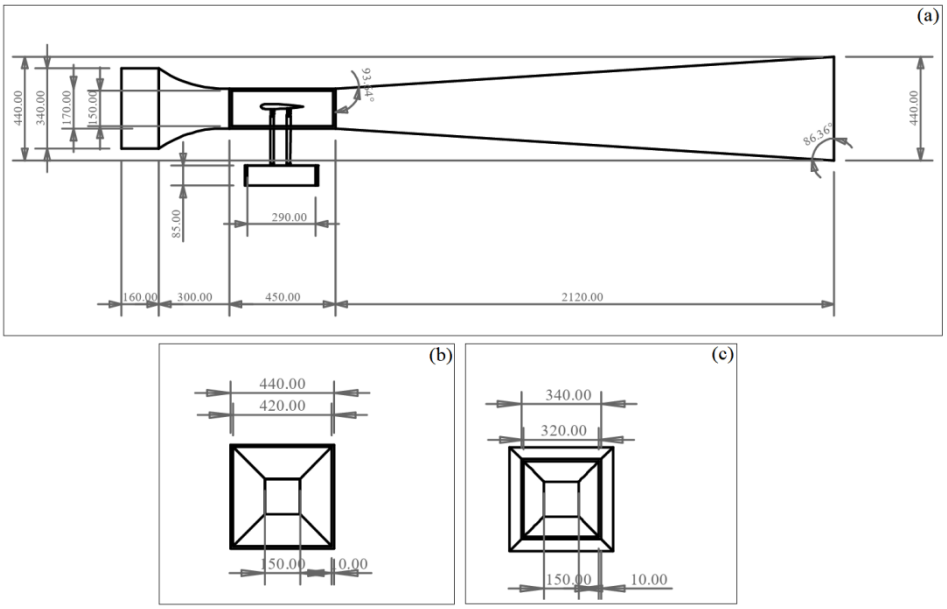

Figure 2. The dimensions of the wind tunnel from different views: (a) side view, (b) left view, (c) right view.

2.1.1. Mini wind tunnel numerical design

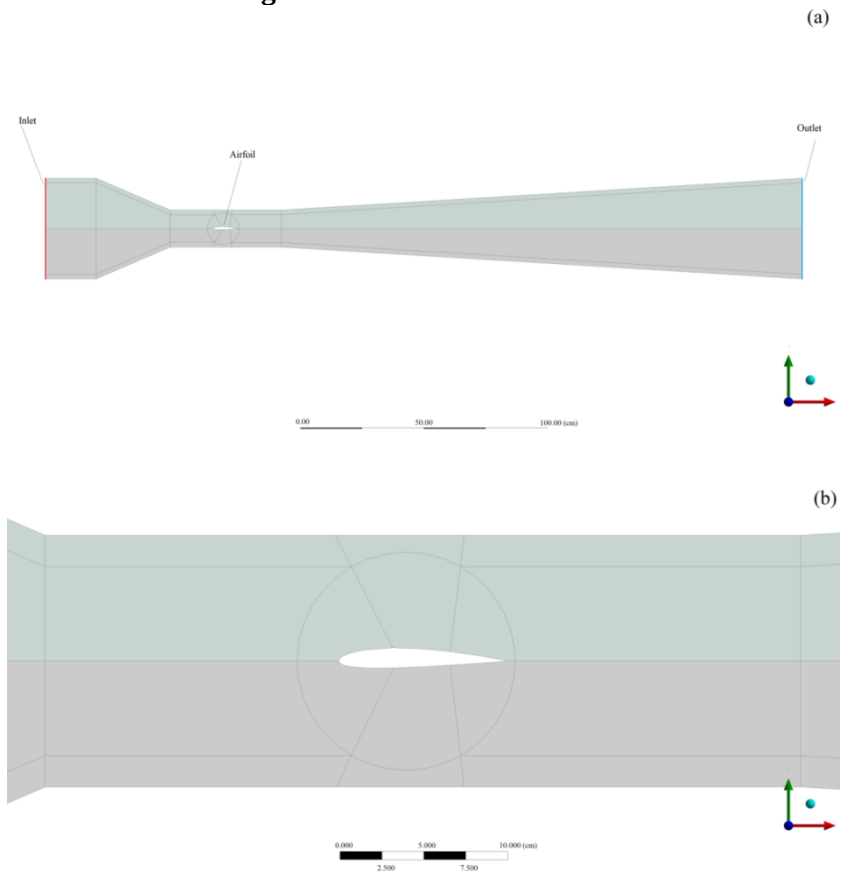

Figure 3. (a) The computational domain in the wind tunnel, (b) close up view of the airfoil in the test section of the wind tunnel

All CFD simulations are performed on a laptop workstation with Intel 8-core (16 threads) i7-11800H CPU, NVIDIA Quadro T600 (4 GB GDDR6) GPU, 64 GB DDR4 RAM. The wind tunnel geometry for the 2D CFD simulations is generated from the XY plane of 3D model shown in Figure 1.a. The computational domain is

subdivided into regions as shown in Figure 3.a to generate a high quality structured mesh. A circular region around the airfoil is divided into six small regions as shown in Figure 3.b to generate an O-type mesh around the airfoil.

Once the regions have been defined, a mesh is generated in the ANSYS Meshing module. Figure 4.a shows the general view of the initially generated moderate mesh. Figures 4.b and 4.c show close-up views of the mesh generated around the airfoil. In the test section region, the computational domain is meshed with structured elements, but an additional triangulation is added outside the O-type mesh. Before conducting CFD analyses, the O-type region surrounding the airfoil is rotated and meshed for each angle of attack, separately. The range is selected in the same way as in the experimental study. The edge mesh size around the airfoil is set to be inflation so that $y^+ < 1$. Mesh independence test for the optimum mesh selection is given in Section 3.1.

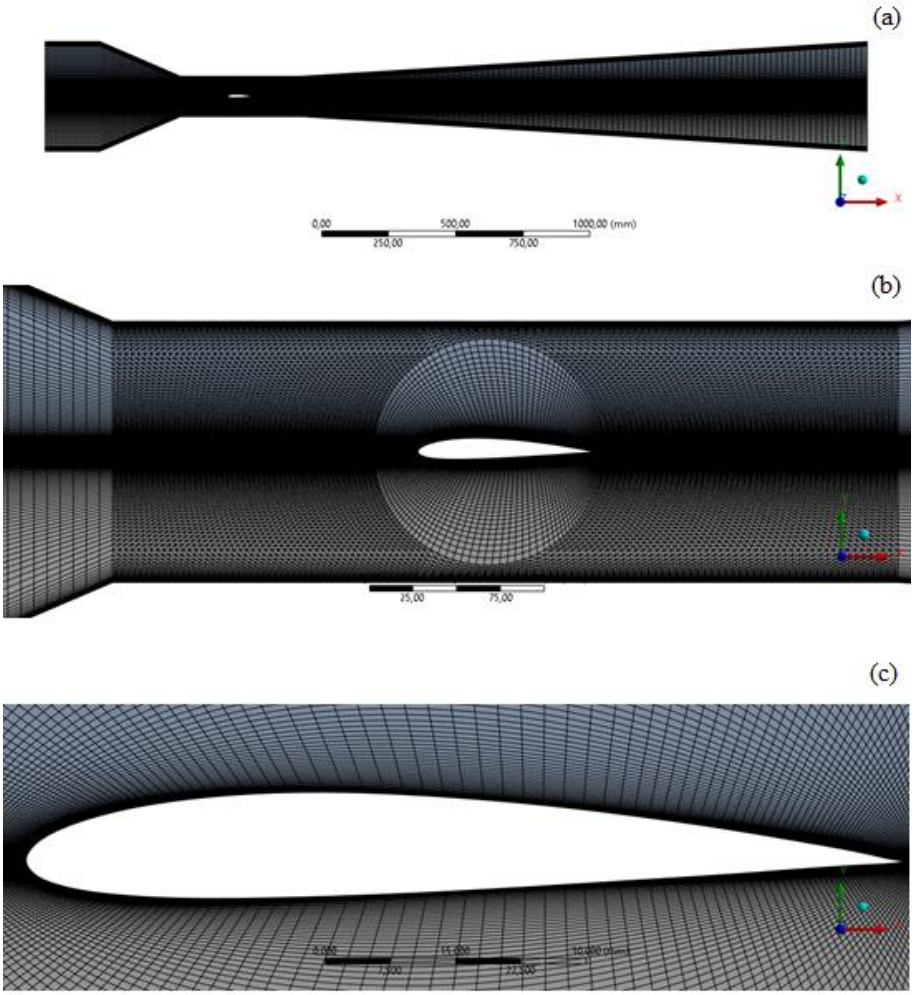

Figure 4. (a) General view of the mesh generated inside the wind tunnel, (b) close up view of the mesh generated inside the test section, (c) close up view of the mesh generated around the NACA 2412 airfoil

2.1.2. Load/balance measurement system design

The design of the load/balance measurement system is inspired by the design of Tintoré (2018), but is more compact and portable. The dimensions of the proposed load/balance measurement system are given in Figure 5. As shown in Figure 6, the measurement system consists of two rollers under the stand, two load cells (load cell-1 and load cell-2) on the stand, connected to the corresponding wing model by vertical rods. The rollers allow the stand to move freely in the longitudinal direction, so that load cell-3 can be used as the drag force measurement module, while the other load cells are used to measure the lift force. The lift force measurement is based on the principle of two load cells working synchronously. The outputs of the load cells, one at the leading edge and the other at the trailing edge of the wing, are processed in Arduino with the effect of the compression force difference and the lift force is calculated. In the same way, drag is measured by capturing the free flow directed motion of the load sensing system balanced on the rollers located under the load cells.

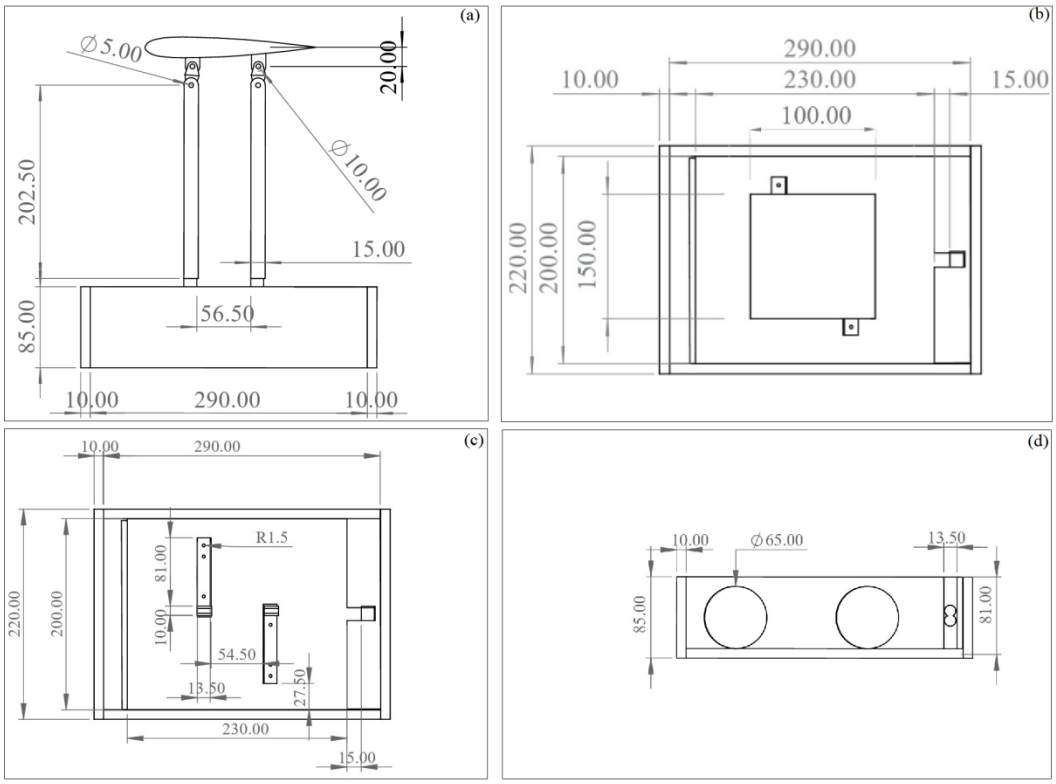

Figure 5. (a) Side view of the load/balance measurement system design (b) top view of the load/balance measurement system design, (c) top view of the load/balance measurement system design (without airfoil), (d)the stationary box enclosing the rollers and one of the load cells.

The following equations are used to measure the lift and drag forces:

$$L = F1 + F2 \quad (1)$$

$$D = F3 \quad (2)$$

Additionally, lift coefficient, C_l and drag coefficient C_d are computed as follows:

$$C_l = \frac{L}{\frac{1}{2}\rho V^2 A} \quad (3)$$

$$C_d = \frac{D}{\frac{1}{2}\rho V^2 A} \quad (4)$$

where ρ is the density [kg/m^3] of air at the inlet of the test section, V is the inlet velocity at the inlet of the test section, A is the planform area [m^2] of the wing.

From CFD calculations, ρ = 1.225 kg/m^3, V = 9 m/s and A = b×c = 0.15×0.1 = 0.015 m^2. In the planform area calculation, b stands for the wing span [m] and c stands for the chord length [m]. Also, Reynolds number in terms of the chord length is found to be 60000 using the following equation:

$$Re = \frac{\rho V c}{\mu} \quad (5)$$

where μ is the kinematic viscosity [Pa.s] of air and is taken as 1.7894×10^{-5} Pa.s.

Sensor data acquisition codes are written using the Ardunio IDE and force measurement experiments are performed at various angles of attack on the NACA2412 airfoil at Reynolds number of 60000, for the maximum flow rate of 5200 m^3/h through the fan controller in the constructed mini wind tunnel.

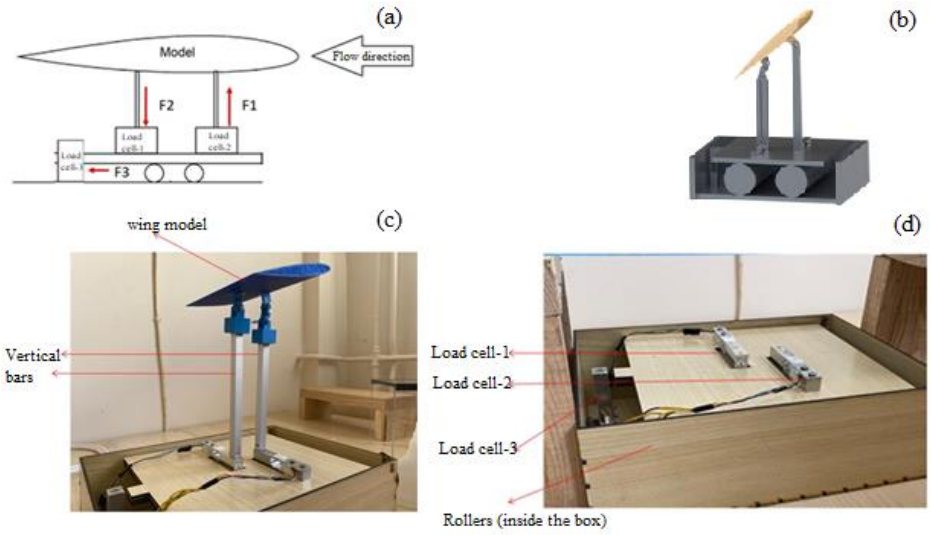

Figure 6. (a) Simplified diagram of the load/balance measurement system design (b) three dimensional design of the load/balance measurement system, (c) manufactured load/balance measurement system with the wing model attached on it, (d) close up view of the placements of the load cells and rollers.

3. Results

In the results section, a mesh independence test is first performed for the computational domain of the mini wind tunnel design. Secondly, the turbulence models, Spalart-Allmaras, Realizable k-ε and SST k-ω are compared for their success in predicting aerodynamic characteristics, i.e. lift and drag, and stall angle of attack. After selecting the most successful turbulence model, a comparison of the CFD results with the experimental results of the current study and similar experimental studies from the literature close to the Reynolds number of the current study is given. Finally, at the end of the results section, the streamlined flow through the wind tunnel is visualized using ANSYS Fluent 2022 R2 (2022).

3.1. Mesh independence test

The first step before proceeding with the CFD solution for the computational domain is to perform a mesh independence test. The meshes are categorized as coarse (Mesh1), moderate (Mesh2), fine (Mesh3) and extra-fine (Mesh4) depending on the number of elements. The sizes are given in Table 1 with their additional informations. For a high quality mesh structure, the minimum orthogonal quality is expected to be greater than 0.1 and the maximum skewness is expected to be less than 0.95 (Ansys Theory Guide, 2022). From tabulated values below, all the meshes produced can be considered to be of good quality.

Figure 7 shows the change in drag and lift coefficients with the number of elements tabulated below. As can be seen from the minimal change in both coefficients for an increase in the number of elements from Mesh3 (175000 elements) to Mesh4 (357000 elements), we conclude that Mesh3 is adequate for the remainder of the study. Also, the last column in Table 1 shows that the y^+ value for both Mesh3 and Mesh4 is less than 1, so both are applicable.

Table 1. Data information for the tested number of elements

Mesh name	Category	Number of elements	Averaga mesh spacing (mm)	Maximum skewness	Minimum orthogonal quality	y^+ value
Mesh1	Coarse	45300	0.200	0.9167	0.1324	1.9604
Mesh2	Moderate	90000	0.100	0.9167	0.1319	1.4909
Mesh3	Fine	175400	0.050	0.9167	0.10635	0.4207
Mesh4	Extra-fine	357000	0.025	0.9167	0.10235	0.4206

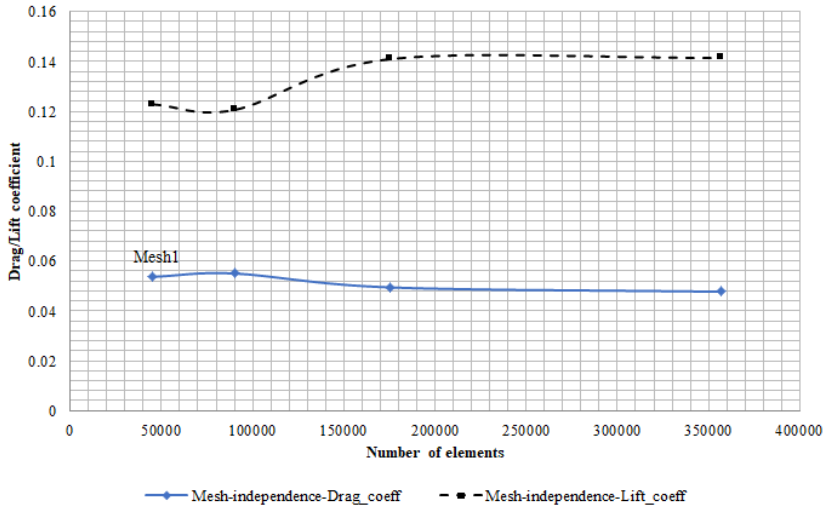

Figure 7. Mesh independence study results for drag coefficient and lift coefficient convergences vs number of elements

3.2. CFD solution compared to experimental results

The pressure-based solver with Spalart-Allmaras, Realizable k-ε and SST k-ω turbulence models are used for the computational domains shown in Figure 4. The SIMPLEC solution method is used in the ANSYS Fluent flow solver and the conservation of mass, conservation of momentum and turbulence equations are solved to a lower bound of 10^{-5} residual. The solutions are generated for a range of geometric angle of attacks, α = -4°, 0°, 4°, 8°, 12°, 16°, 18° and 20°.

Figure 8 shows the lift coefficient, C_l, and drag coefficient, C_d, distributions for the NACA 2412 airfoil at Re = 60000 over the range of angles of attack between -4º and 20º. For low angles of attack between -4º and 4º C_l the predictions of the turbulence models do not differ. Spalart-Allmaras and realizable k-ε turbulence models differ only in their stall angles of attack. Realizable k-ε turbulence models give more realistic high stall angle of attack than other turbulence models, similar to the experimental results. The C_d predictions of the turbulence models do not change much, only SST k-ω gives small fluctuations in the moderate angle of attack. The values are tabulated and compared with the current experimental study in Tables 2 and 3. As can be seen in the total average error column and Equations 6 and 7 below, this turbulence model will be used as a comparable CFD study for the experimental data in the following paragraphs.

$$E_l = \frac{\sum_{\alpha=-4^\circ}^{20^\circ}[C_{l,e}(\alpha) - C_l(\alpha)]}{8} \quad (6)$$

$$E_d = \frac{\sum_{\alpha=-4^\circ}^{20^\circ}[C_{d,e}(\alpha) - C_d(\alpha)]}{8} \quad (7)$$

Table 2. Comparison of C_l values for the selected turbulence models with experimental study

Turb. Model \ α	-4º	0º	4º	8º	12º	16º	18º	20º	E_l, Total average error
Spalart-Allmaras	-0.431	0.187	0.584	0.919	1.090	1.212	1.204	1.135	-0.139
Realizable k-ε	-0.547	0.119	0.457	0.741	0.894	1.178	1.151	0.993	-0.025
SST k-ω	-0.403	0.182	0.610	0.815	1.111	1.205	1.329	1.157	-0.151
Exp. Study, $C_{l,e}$	-0.272	0.030	0.610	0.697	0.882	0.925	1.012	0.903	-

Table 3. Comparison of C_d values for the selected turbulence models with experimental study

Turb. Model \ α	-4°	0°	4°	8°	12°	16°	18°	20°	E_d, Total average error
Spalart-Allmaras	0.034	0.024	0.029	0.043	0.078	0.241	0.406	0.428	0.239
Realizable k-ε	0.090	0.056	0.057	0.074	0.111	0.251	0.467	0.439	0.206
SST k-ω	0.152	0.018	0.064	0.037	0.156	0.314	0.632	0.471	0.169
Exp. Study, $C_{d,e}$	0.269	0.134	0.269	0.349	0.403	0.443	0.564	0.766	-

As the mesh independence tests have been successfully generated and there is no divergence for any of the angles of attack, it is unlikely that the large errors at angle of attacks of -4°, 0°, 4° lies with the mesh quality or the numerical solution technique. However, it may be related to the vertical bars attached under the wing and the walls enclosing the wind tunnel test section. The drag is increased by the additional body of the vertical bars' cross-sections at low angles of attack, specifically between -4° and 4°. Additionally, these extra components significantly reduce lift at the same angle of attack due to their less aerodynamic shape. Nonetheless, the overall presentation of the C_l vs α and C_d vs α curves in Figure 8 is unaffected, especially at the critical stall angle of attack, 18° and post-stall angle of attack, 20°.

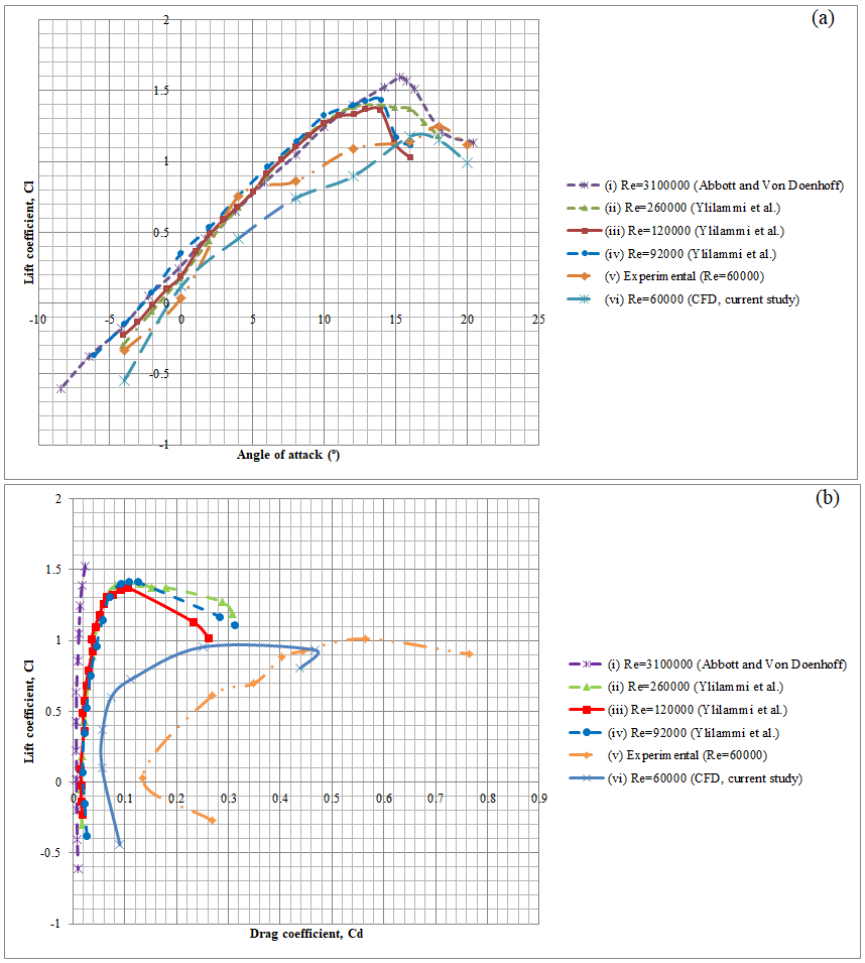

Figure 8. Comparison of lift coefficient, C_l (a) vs angle of attack, α, and (b) vs drag coefficient, C_d for experimental results of (i) Abbott et al. (1945) at Re =3100000, (ii) Ylilammi et al. (2010) at Re = 260000, (iii) Ylilammi et al. (2010) at Re = 120000, (iv) Ylilammi et al. (2010) at Re = 92000 with (v) current experimental study at Re = 60000 and (vi) current CFD study at Re = 60000 around the NACA 2412 airfoil

The current study is generated both numerically and experimentally for a low Reynolds number flow of 60000 around a small scale (c = 0.1m) NACA 2412 airfoil profile wing. Figure 8 examines a wide range of Reynolds numbers for the flow around NACA 2412, varying from 92000 (Ylilammi et al., 2010) to 310000 (Abbott et al., 1945) from the literature. As can be seen in Figure 8.a, a similarity between the reference studies and the current study is captured for angles of attack between -4º and 4º. After moderate angles of attack, i.e. higher than 4º, the C_l curve cannot rise to higher values, but this is an expected result since the Reynolds number is very much lower than in the reference studies. Looking at the differences between the experimental and CFD study of C_l, the stall angle of attack is slightly different between 16º and 18º but at the same level of C_l, 1.2 to 1.25. Thus, it can be concluded that the realizable k-ε turbulence model can be considered as a successful model to predict the change of C_l with α. Looking at Figure 8.b, the variation of C_d with C_l is also comparable with reference studies, but the drag effect for the reference studies is higher for the same C_l values as expected. In conclusion, the NACA 2412 airfoil profile wings are more efficient for the medium to high Reynolds numbers and the constructed load/balance measurement system and mini wind tunnel are successful in terms of C_l and C_d measurements.

The velocity contours of the flow inside the wind tunnel and the close-up view of the test section with the NACA 2412 airfoil in it are shown in the following figures for the selected turbulence model, realizable k-ε turbulence model.

In Figure 9, at α = -4°, velocity contours are nearly the same in the settling chamber and collector section so that the wind tunnel design fulfills the uniform flow expectations for these sections. Additionally, realizable k-ε turbulence model displays the separation from the leading edge through wake region as expected.

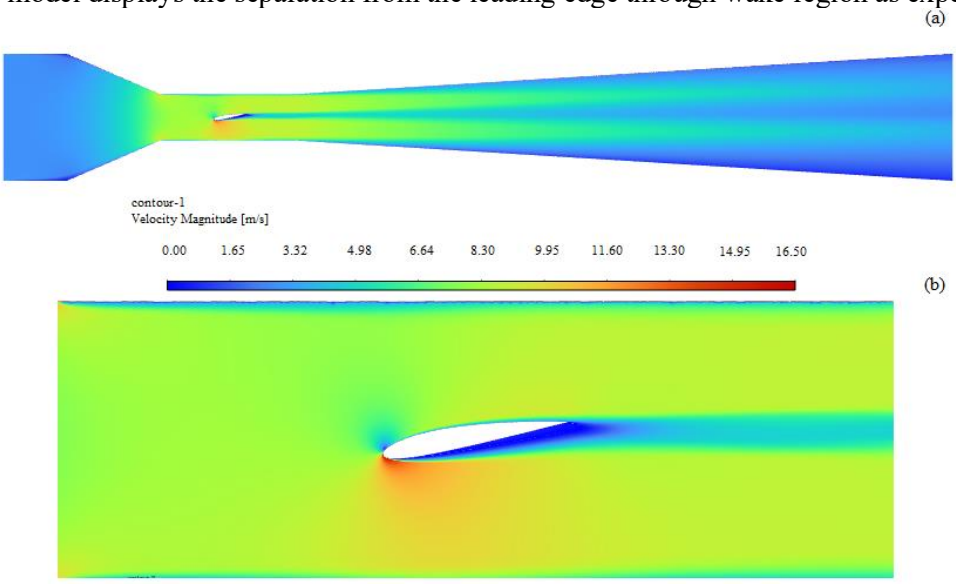

Figure 9. Velocity contours (a) inside the virtual wind tunnel and (b) around the NACA 2412 airfoil, α = -4°, Re = 60000, realizable k-ε turbulence model

At angle of attack, α = 0°, the velocity contours differ between settling chamber to test section from 2.10 m/s to 10.50 m/s as shown in Figure 10. At angle of attack, α = 4°, as seen in Figure 11 the contours show a realistic separation behavior near the trailing edge.

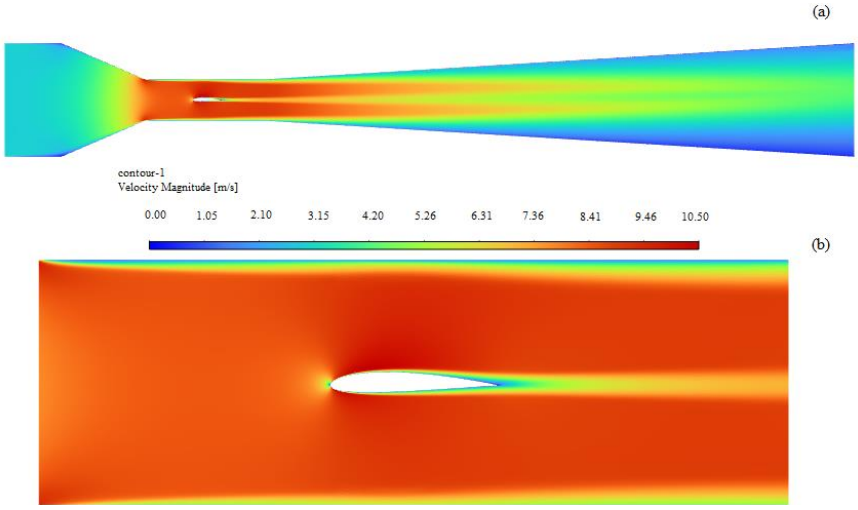

Figure 10. Velocity contours (a) inside the virtual wind tunnel and (b) around the NACA 2412 airfoil, α = 0°, Re = 60000, realizable k-ε turbulence model

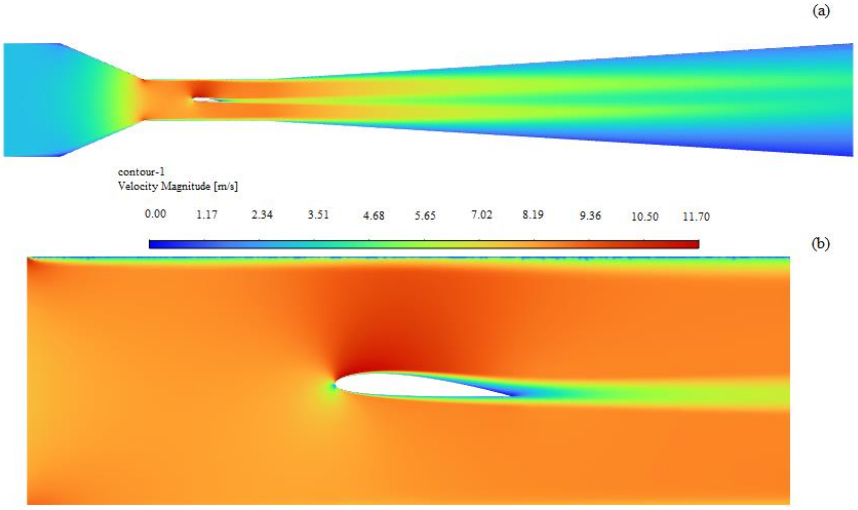

Figure 11. Velocity contours (a) inside the virtual wind tunnel and (b) around the NACA 2412 airfoil, α = 4°, Re = 60000, realizable k-ε turbulence model

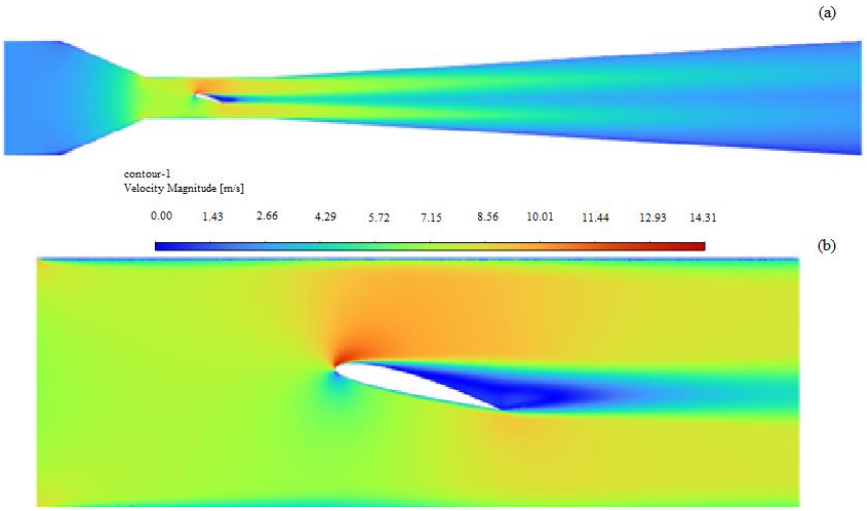

Figure 12. Velocity contours (a) inside the virtual wind tunnel and (b) around the NACA 2412 airfoil, α = 8°, Re = 60000, realizable k-ε turbulence model

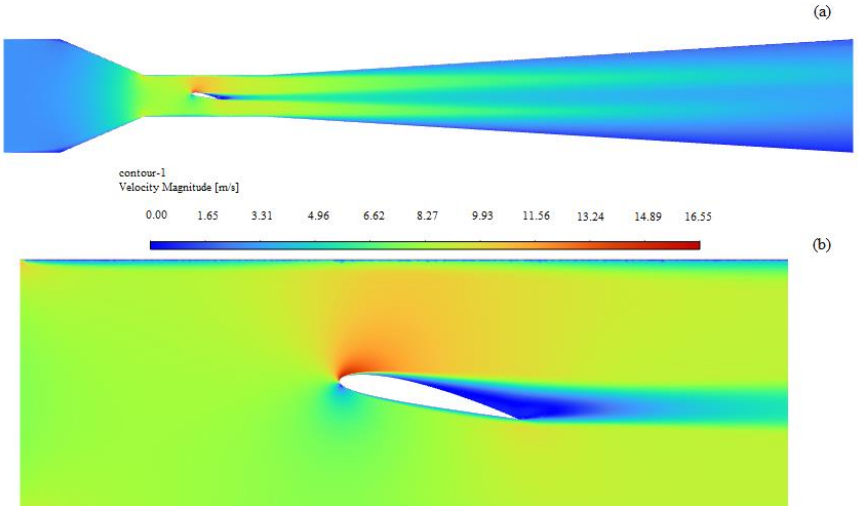

Figure 13. Velocity contours (a) inside the virtual wind tunnel and (b) around the NACA 2412 airfoil, α = 12°, Re = 60000, realizable k-ε turbulence model

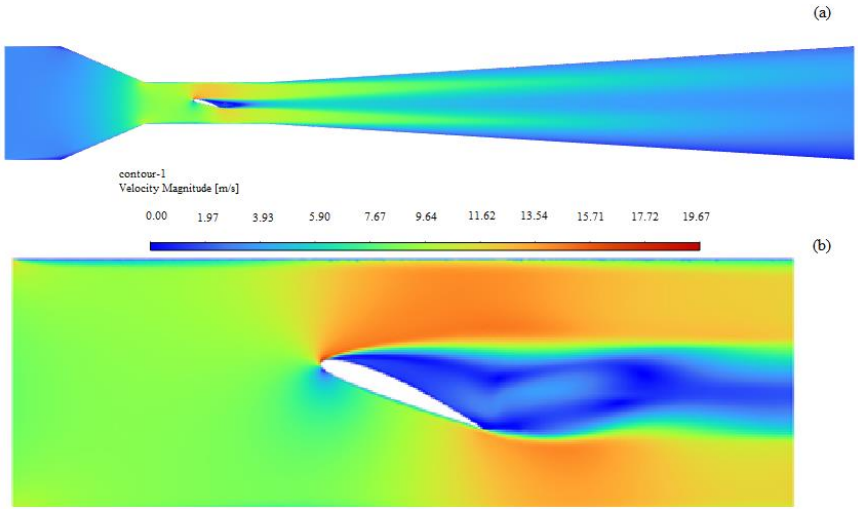

Figure 14. Velocity contours (a) inside the virtual wind tunnel and (b) around the NACA 2412 airfoil, α = 16°, Re = 60000, realizable k-ε turbulence model

At angle of attack, α = 8°, the realizable k-ε turbulence model exhibit leading edge separation and a uniform wake region as shown in Figure 12. At angle of attack, α = 12°, realizable k-ε turbulence model gives a good prediction of separation location over the upper surface in Figure 13.b.

At angle of attack, α = 16°, realizable k-ε turbulence model predict the vortex shedding at the wake region in Figure 14, successfully. At high angle of attacks 18º and 20º, in Figures 15 and 16, respectively, the case study with realizable k-ε model continues to show the vortex shedding behavior in the wake region as expected.

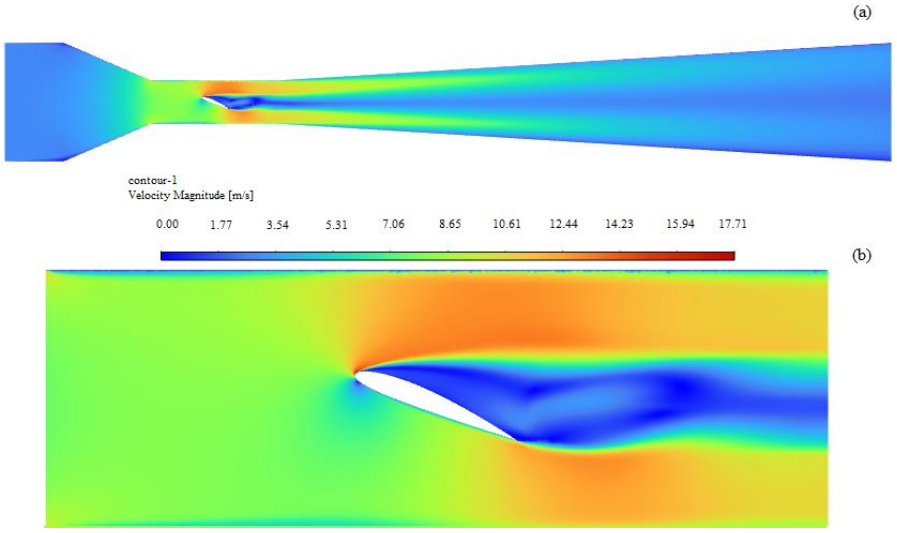

Figure 15. Velocity contours (a) inside the virtual wind tunnel and (b) around the NACA 2412 airfoil, α = 18°, Re = 60000, realizable k-ε turbulence model

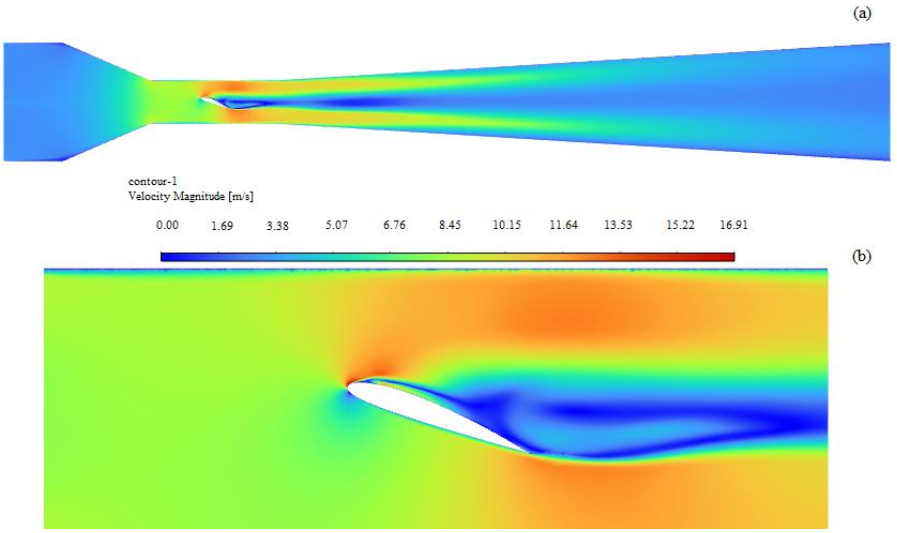

Figure 16. Velocity contours (a) inside the virtual wind tunnel and (b) around the NACA 2412 airfoil, α = 20°, Re = 60000, realizable k-ε turbulence model

4. Conclusion

In this study, a portable three-axis load/balance measurement system in a mini wind tunnel is investigated both numerically and experimentally. A low-cost, portable and compact three-axis load/balance measurement system that can be adapted and used in wind tunnels of different sizes and characteristics is constructed for future academic use.

As a result of the mesh independence test, a mesh of 175000 elements is found to be sufficient for the current numerical (virtual) wind tunnel design. Realizable k-ε turbulence model gives more realistic high stall angles of attack than other turbulence models, similar to experimental results. Numerically, the best C_l prediction (an average error of -0.025) is generated by the realiziable k-ε turbulence model, and it came second (an average error of 0.206) in the C_d prediction. Using this turbulence model, the overall representation of the C_l vs α and C_d vs α curves is successful, especially at the critical stall angle of attack of 18º and the post-stall angle of attack of 20º.

In addition to the current experimental study, four other literature studies in similar Reynolds number ranges are used as reference cases. A similarity between the reference studies and the current study is found for angles of attack between -4º and 4º. After moderate angles of attack, i.e. higher than 4º, the C_l curve cannot rise to

higher values, but this is an expected result since the Reynolds number is very much lower than in the reference studies. Looking at the differences between the experimental and CFD study of C_l, the stall angle of attack is slightly different between 16º and 18º, but at the same level of C_l, 1.2 to 1.25. The variation of C_d with C_l is also comparable to the reference studies, but the drag effect for the reference studies is higher for the same C_l values.

A visual study of the flow around the NACA 2412 airfoil is given as velocity contours in addition to the numerical comparisons. At an angle of attack of $\alpha = 0°$, the velocity contours vary from 2.10 m/s to 10.50 m/s between the settling chamber and the test section. The contours show a realistic separation behaviour near the trailing edge at an angle of attack of $\alpha = 4°$. At an angle of attack of $\alpha = 8°$, the realizable k-ε turbulence model shows leading edge separation and a uniform wake region. At an angle of attack of $\alpha = 12°$, the model gives a good prediction of the separation location over the upper surface. At an angle of attack of $\alpha = 16°$, the model successfully predicts the vortex shedding in the wake region. At high angles of attack, 18° and 20°, the case study continues to show the vortex shedding behaviour in the wake region as expected.

From the numerical and experimental results, it is concluded that the NACA 2412 airfoil profile wings are more efficient for moderate to high Reynolds numbers and the constructed load/balance measurement system and mini wind tunnel are highly successful in terms of C_l and C_d measurements.

Acknowledgement

This work is financially supported by the Scientific Research Project Fund (BAP) of GAZİANTEP UNIVERSITY under the project number HUBF.ÖKAP.22.01. The 3D printing and laser cutting processes are completed at the IOM FabLab Application Center, Gaziantep Office.

Author contribution

The contribution role of E. Kara includes conceptualization, data curation, formal analysis, funding acquisition, investigation, methodology, project administration, supervision, validation, visualization, writing – original draft, and writing – review & editing. The contribution role of K. Öztürk includes data curation, formal analysis, investigation, and writing first part of the original draft.

Declaration of ethical code

The authors of this article declare that the materials and methods used in this study do not require ethics committee approval and/or legal-special permission.

Conflicts of interest

No potential conflict of interest was reported by the authors.

References

Abbott, I. H., Von Doenhoff, A. E., & Stivers Jr, L. (1945). *Summary of airfoil data (No. NACA-TR-824)*. https://ntrs.nasa.gov/api/citations/19930090976/downloads/19930090976.pdf

ANSYS Fluent Theory Guide (2022, July). https://ansyshelp.ansys.com/Views/Secured/corp/v222/en/pdf/Ansys_Fluent_Theory_Guide.pdf

ANSYS Fluent User's Guide (2022, July). https://ansyshelp.ansys.com/Views/Secured/corp/v222/en/pdf/Ansys_Fluent_Users_Guide.pdf

Ate AEROTECH - 3 Component External Wind Tunnel Balances. (2024, January 11). http://www.ate-aerotech.co.uk/capabilities/aerodynamic-test-equipment/external-balances/3-component-external-wind-tunnel-balances

Barlow, J. B., Rae, W. H., & Pope, A. (1999). *Low-speed wind tunnel testing* (3rd ed.). John Wiley & Sons.

Fernandes, J. T. (2018). *Design of a wind tunnel force balance* [Master's thesis, Technical University of Lisbon].

Koca, M. S. (2019). *Su tünellerinde model hareket kontrolü ve senkron aerodinamik kuvvet ölçüm sistemi tasarımı* [Master's thesis, Başkent University Institute of Science].

Kumar, R., Srivatsa, B. R., & Subramanian, B. (2021). Calibration design evaluations through computational analysis and investigation of a six-component wind tunnel balance. *ISSS Journal of Micro and Smart Systems*, *10*, 7-31.

Portman, V., Sandler, B. Z., Chapsky, V., & Zilberman, I. (2009). A 6-DOF isotropic measuring system for force and torque components of drag for use in wind tunnels: Innovative design. *International Journal of Mechanics and Materials in Design, 5*, 337-357. https://doi.org/10.1007/s10999-009-9106-6

Randers-Pehrson, N. (1935). Pioneer wind tunnels. *Smithsonian Miscellaneous Collections*.

Samardžić, M., Anastasijević, Z., Marinkovski, D., Ćurčić, D., & Isaković, J. (2014). External six-component strain gauge balance for low speed wind tunnels. *Scientific Technical Review, 64*(3), 40-46. https://doi.org/10.1007/s10999-009-9106-6

Stewart, D. (1965). A Platform with six degrees of freedom. *International Journal of Mechanics and Materials in Design Proceedings of the Institute of Mechanical Engineers, 180*(1), 371-386. https://doi.org/10.1243/PIME_PROC_1965_180_029_02

Tintoré, I. B. (2018). *Design of a Three-axis Wind Tunnel Force Balance* [Bachelor's thesis, University of Zagreb Faculty of Transport and Traffic Sciences].

Tomin, M., Scipioni, M., & Gatti, B. (2020). Design, Construction and Testing of a 3-Component Force Balance for Educational Wind Tunnels in Undergraduate Aerodynamics. *Journal of Aviation/Aerospace Education & Research, 29*(1), 89-105.

Ylilammi, N., Cavalieri, A. V. B., & Soinne, E. (2010). Experimental and computational study of two flapped airfoils at low Reynolds Numbers. 27th Congress of the International Council of the Aeronautical Sciences (ICAS) (pp. 1-9), Nice, France.